

# Fix your downsampling ASAP!

## Be natively more robust via Aliasing and Spectral Artifact free Pooling

Julia Grabinski  
 Fraunhofer ITWM, Kaiserslautern  
 Visual Computing, University of Siegen  
 julia.grabinski@itwm.fraunhofer.de

Janis Keuper  
 Fraunhofer ITWM, Kaiserslautern  
 IMLA, Offenburg University

Margret Keuper  
 Visual Computing, University of Siegen  
 Max Planck Institute for Informatics, Saarbrücken

### Abstract

Convolutional neural networks encode images through a sequence of convolutions, normalizations and nonlinearities as well as downsampling operations into potentially strong semantic embeddings. Yet, previous work showed that even slight mistakes during sampling, leading to aliasing, can be directly attributed to the networks' lack in robustness. To address such issues and facilitate simpler and faster adversarial training, [12] recently proposed FLC pooling, a method for provably alias-free downsampling - in theory. In this work, we conduct a further analysis through the lens of signal processing and find that such current pooling methods, which address aliasing in the frequency domain, are still prone to spectral leakage artifacts. Hence, we propose aliasing and spectral artifact-free pooling, short ASAP. While only introducing a few modifications to FLC pooling, networks using ASAP as downsampling method exhibit higher native robustness against common corruptions, a property that FLC pooling was missing. ASAP also increases native robustness against adversarial attacks on high and low resolution data while maintaining similar clean accuracy or even outperforming the baseline.

### 1. Introduction

Compressing data to achieve more sparse representations is a widely employed technique in current Convolutional Neural Network (CNN) architectures. In this regard, standard methods such as MaxPooling, Average Pooling, or Convolution with a stride of two are commonly used. However, all of these methods suffer from a significant drawback, which is their susceptibility to aliasing [13, 41, 42].

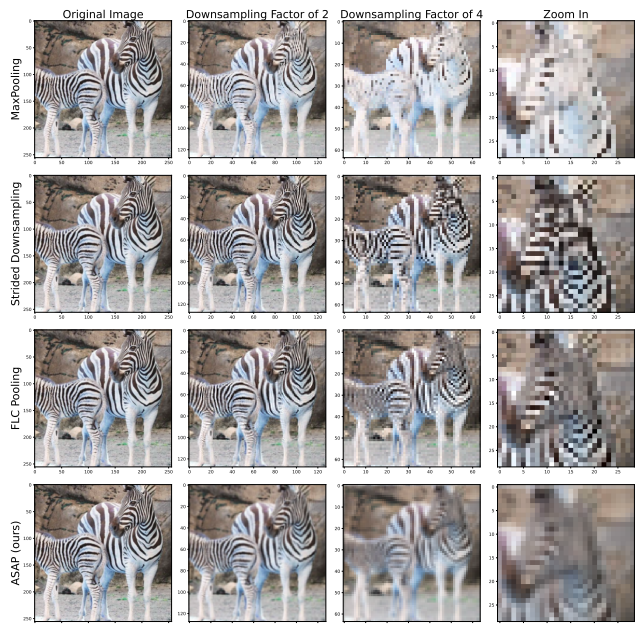


Figure 1. We compare the influence of downsampling by different methods. The first row shows the commonly used MaxPooling and the second row shows strided downsampling. In the third row we use FLC Pooling [12] for downsampling and in the last row we show our new aliasing and spectral artifact-free downsampling. While MaxPooling defaces the important object, the zebra, FLC Pooling and our ASAP preserve the zebra. However, FLC Pooling suffers from spectral artifacts which can occur after the transformation from the spectral to the spatial domain. Especially after the first two downsampling operations these artifacts get visible around the head of the zebra.

Previous research has demonstrated a close relationship between vulnerability to aliasing and the network's robust-

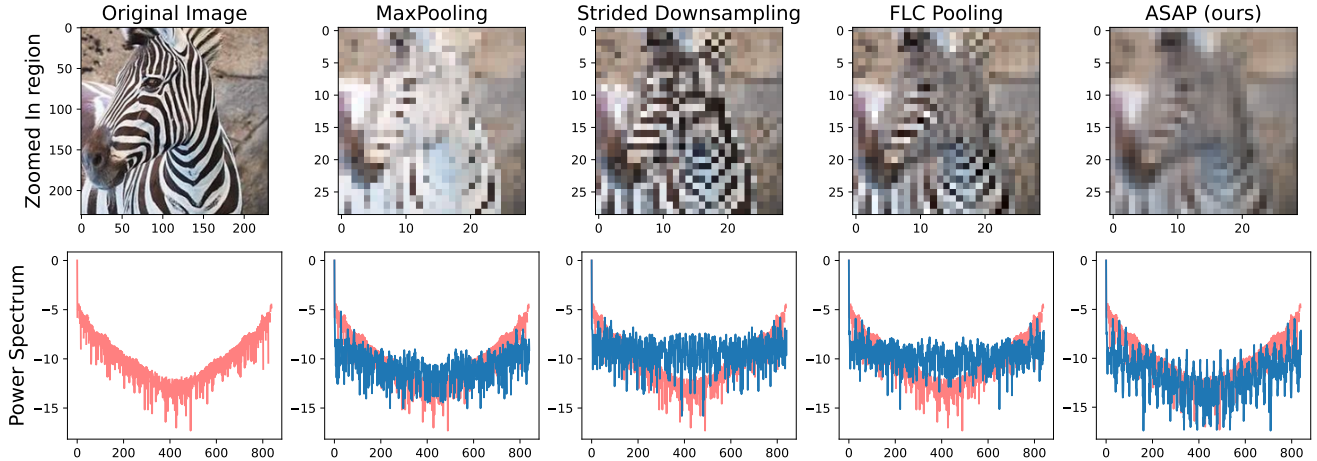


Figure 2. Different power spectra after various downsampling methods as well as the actual downsampled images. The first row shows the original images as well as the downsampled versions with different pooling methods. After MaxPooling the zebra’s fur structures are much less recognizable. When simple downsampling via stride is applied, grid structures appear, and we observe aliasing artifacts. Using FLC pooling [12] reduces these aliasing artifacts. However, ringing artifacts surrounding the zebra’s head get visible. Only our ASAP is able to downsample the image without artifacts. The second row presents the power spectrum (in log scale for the y-axis, x-axis presents the frequency bands) of the images. The first column represents the original power spectrum of the image. Underlying each power spectrum of the downsampled versions we plotted the spectrum of the original image in red. Our ASAP is the only method to achieve a similar power spectrum to the original image.

ness [13, 41]. Consequently, prior approaches have suggested using blurring kernels to mitigate aliasing [41, 42], or downsampling in the frequency domain to achieve aliasing-free downsampling [12]. This results in higher robustness of the networks against common corruptions [16] and even adversarial attacks [12] like [9, 25, 2]. Nonetheless, these methods are still prone to other spectral artifacts, such as visible ringing artifacts in the spatial domain.

We demonstrate that the manner in which images, feature maps, or signals are downsampled can result in undesired artifacts. While there has been extensive research on the topic of aliasing artifacts in CNNs [13, 41, 42], other types of spectral leakage artifacts related to downsampling in CNNs have not been thoroughly explored. Therefore, our objective is to investigate whether downsampling methods like FLC pooling [12], which are known to be aliasing-free, are also generally free from other types of artifacts.

Our findings indicate that this is not the case. Even though FLC pooling is designed to be aliasing-free, it still exhibits spectral leakage artifacts, which manifest as ringing artifacts. An example of such artifacts can be observed in 1, specifically in the third row and third column, where the structures near the zebra’s head are repeated in a rippled manner. In contrast, the standard downsampling method used in many CNN architectures, like MaxPooling, completely distorts the zebra’s structure. Whereas strided downsampling results in severe aliasing artifacts, visible as grid structures on the fur of the zebra. Consequently, it is crucial to reevaluate the choice of downsampling techniques

employed within CNNs.

Our contributions are as follows:

- We visually justify why current downsampling methods like MaxPooling and Striding should be replaced by downsampling methods which are more conform with signal processing fundamentals.
- Further, we investigate aliasing free downsampling, FLC pooling [12] and reveal that it is still prone to spectral leakage artifacts.
- Consequently, we introduce **Aliasing and Spectral Artifacts-free Pooling**, short ASAP. Hereby, we achieve higher native robustness compared to state-of-the-art models and the aliasing free FLC pooling [12].
- To validate the native robustness of our ASAP, we empirically evaluate against adversarial attack [9, 25, 2] as well as common corruptions incorporated in ImageNet-C [16].
- Moreover, we combine our ASAP with simple FGSM adversarial training [9] and show that the resulting models achieve superior performance in terms of clean and robust accuracy.

## 2. Related Work

### 2.1. Anti-Aliasing

The issue of aliasing effects in CNN-based neural networks has been extensively explored in the literature from

various perspectives. In [41], the authors enhance the shift-invariance of CNNs by incorporating anti-aliasing filters implemented as convolutions. Building upon this work, [42] further improve shift invariance by utilizing learned blurring filters instead of predefined ones. In [26], the pooling operations leverage the low-frequency components of wavelets to mitigate aliasing and enhance robustness against common image corruptions. [19] introduces a depth adaptive blurring filter before pooling, along with an anti-aliasing activation function. The importance of anti-aliasing is also recognized in the field of image generation. [22] suggests the use of blurring filters to eliminate aliases during image generation in generative adversarial networks (GANs), while [5] and [21] incorporate additional loss terms in the frequency domain to address aliasing. In [13], the authors empirically demonstrated that adversarially robust models exhibit lower levels of aliasing in their down-sampling layers compared to non-robust models, using a proposed aliasing measure. Motivated by these findings, [12] propose an aliasing-free downsampling method in the frequency domain to prevent catastrophic overfitting. In extension, we present a novel approach achieving not only aliasing-free downsampling but also spectral leakage artifact-free downsampling for native robustness.

## 2.2. Spectral Leakage Artifacts

The issue of spectral leakage artifacts, including the specific case of aliasing artifacts, has received relatively less attention in the context of CNNs. These spectral leakage artifacts often arise when applying finite windows to infinite signals, as demonstrated in [12]. These artifacts manifest as ringing artifacts in the spatial domain, as described in [8], and are associated with the Gibbs phenomenon [14]. To mitigate these spectral leakage artifacts, various window functions can be employed, as discussed in [27].

In the field of digital image processing, the use of 2D window functions is prevalent, particularly in biomedical image processing where window functions play a crucial role in spectral analysis [20, 33].

More recently, [35] investigated spectral leakage artifacts within CNNs and found that the use of small kernels can contribute to such artifacts. Consequently, they propose learning larger kernels while also applying a Hamming window to the convolutional weights as a solution.

## 2.3. Robustness

**Common Corruptions.** The robustness of CNNs can be assessed from various perspectives. One aspect involves evaluating their resilience against common corruptions caused by factors such as diverse weather conditions, varying lighting conditions, or subpar camera quality. To measure this kind of robustness, the widely recognized ImageNet-C dataset is utilized [16]. This dataset aims to simulate

real-world scenarios through synthetic means. Approaches that target this form of robustness often employ data augmentation techniques [17, 3]. Other methods include shape biasing [7] or combining adversarial training with augmentations [23].

**Adversarial Attacks.** In contrast to common corruptions, which involve fixed alterations applied to the dataset, adversarial attacks expose network-specific vulnerabilities. These attacks are designed to deceive a network and can operate under different conditions. In a white box attack, the attacker has full access to the network’s architecture and parameters, while in a black box attack, the attacker only has access to the network’s outputs.

In any case, a CNN should demonstrate reliability and resist being fooled by adverse weather conditions, varying camera settings, or deliberately crafted adversarial inputs.

## 2.4. Adversarial Training

To establish robustness against adversarial attacks, various defense methods have been developed. One effective approach is adversarial training (AT) [9, 30], which involves training the network with adversarial examples. These adversarial samples are incorporated by introducing an additional loss term during network training [6, 40]. Other techniques include utilizing additional training data [1, 32], particularly the *ddpm* dataset [11, 28, 29], which consists of one million extra samples for CIFAR-10 and is generated using the model proposed by [18]. Data augmentation has also proven to enhance adversarial robustness [10], and combining it with weight averaging further improves performance [29]. Some more advanced techniques involve adding specifically generated images to the training dataset [11].

However, a major drawback of most AT methods is the significant increase in computational resources required for training. Generating adversaries during training alone can increase training time by a factor of seven to fifteen [25, 36, 38, 40]. Adding additional data or generating new images [11] would further amplify the computational burden.

Therefore, utilizing a simple adversary without the need for additional data is preferable. The Fast Gradient Sign Method (FGSM) [9] is the simplest form of adversary, as it creates adversaries in a single step, making it more efficient than more complex methods like Projected Gradient Descent (PGD) [25], which require multiple steps to generate adversaries. This iterative process of PGD takes nearly eight times longer than simple FGSM training. However, FGSM is susceptible to catastrophic overfitting [37], where the robust accuracy drops to zero against more complex adversaries (e.g., PGD) when trained with simpler adversaries (e.g., FGSM), while still maintaining high accuracy against simple adversaries. [13] demonstrated a correlation between aliasing after downsampling and catastrophic over-

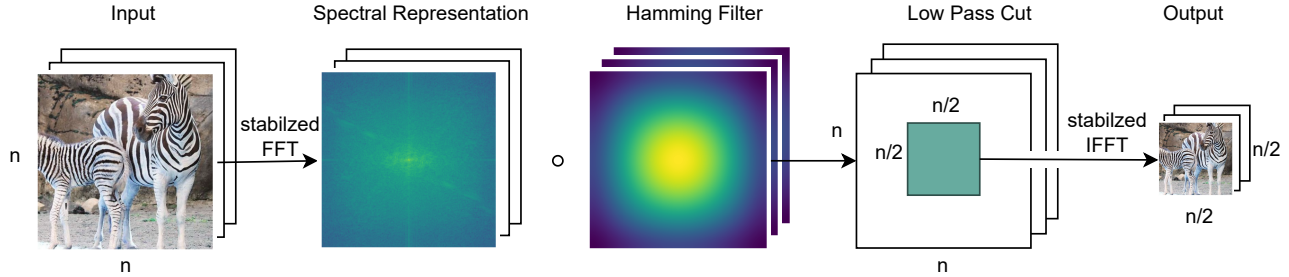


Figure 3. Our aliasing and spectral artifact-free downsampling, short ASAP. First, we transform the input with our stabilized FFT into the frequency domain and shift the low-frequency components in the middle. Afterwards, we apply a hamming filter on our frequency representation to prevent spectral leakage artifacts. Further, we apply frequency low cut pooling [12] to downsample aliasing-free. Lastly, we transform back into the spatial domain via our stabilized IFFT.

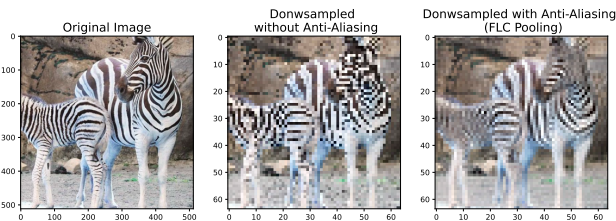


Figure 4. Example of aliasing after standard downsampling via stride compared to current anti-aliasing methods like FLC pooling [12]. Downsampling via stride incorporates severe grid artifacts aka. aliasing artifacts.

fitting, proposing FLC pooling [12] as a solution to mitigate catastrophic overfitting.

### 3. Aliasing- and Spectral Artifacts-Free Pooling

We present a novel approach called Alias and Spectral Artifact-free Pooling (ASAP), which addresses not only the well-known issue of aliasing [12, 41, 42], but also tackles other types of spectral leakage artifacts.

Spectral leakage artifacts occur when finite window operations are applied to infinite signals or when infinite window functions are used on finite signals. These artifacts manifest as ringing artifacts, which can be explained by the equivalence between a box function and a sinc function in both the spectral and spatial domains.

Aliasing artifacts are a specific type of spectral leakage artifact that occurs when a signal is improperly sampled at a rate below twice the signal’s bandwidth [34]. This leads to the overlapping of high-frequency components with low-frequency components, making them indistinguishable. In the spatial domain, this frequency domain overlap becomes visible as grid-like artifacts.

**Aliasing-free Downsampling.** Previous approaches have introduced downsampling methods that aim to suppress aliasing by applying blurring techniques before downsam-

pling [41, 42], or by directly removing aliases in the frequency domain through the removal of low-frequency components to prevent the folding of high-frequency components (aliasing) [12].

Blurring methods [41, 42] are unable to completely eliminate aliasing, resulting in low robustness and catastrophic overfitting during adversarial training [12], similar to standard networks. On the other hand, the approach of cutting out low-frequency components [12] has shown promise in preventing catastrophic overfitting. To implement this type of downsampling, the feature maps of the networks are transformed into the frequency domain using Fast Fourier Transform (FFT). Subsequently, the low-frequency components are shifted to the center (as depicted in the first step of Figure 3). This allows for the application of a rectangular function ranging from  $1/4N$  to  $3/4N$ , where  $N$  represents the width and height of the feature map in the shifted spectral representation (Low Pass Cut in Figure 3). This region contains only low-frequency information within  $1/2B$ , where  $B$  denotes the bandwidth of the signal, resulting in aliasing-free downsampling<sup>1</sup>.

However, these methods are still susceptible to artifacts, although not typical aliasing artifacts (visible as grid artifacts). Instead, these artifacts manifest as spectral leakage artifacts, which exhibit a sinc-like structure.

**Spectral Artifact-free Transformation.** To achieve completely aliasing-free downsampling, it is necessary to apply the rectangular function in the frequency domain. However, this operation, when combined with the transformation back into the spatial domain, can introduce sinc artifacts in the spatial representation. To mitigate such artifacts, it is essential to apply a filter that smoothens the sharp edges of the rectangular function. Therefore, we propose the use of a Hamming window ( $H(n)$ ), which is defined for 1D signals

<sup>1</sup>For more detailed information, please refer to [12].

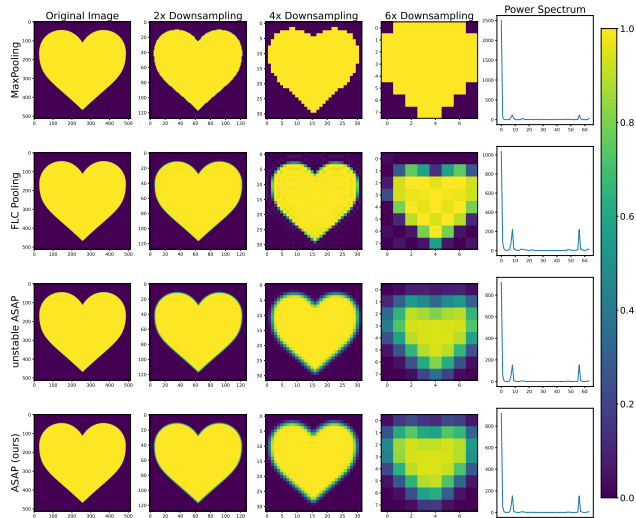


Figure 5. We compare the influence of downsampling by different methods. The first row shows the commonly used MaxPooling. In the second row we use FLC Pooling [12] for downsampling and in the last two rows we show our new aliasing and spectral artifact-free downsampling, where the third row shows the unstable version and the last row our stable ASAP. Additionally, we plot the power spectrum of each downsampled heart in the last column.

as follows:

$$H(n) = \alpha - (1 - \alpha) \cdot \cos\left(\frac{2n\pi}{N}\right), \quad 0 \leq n \leq N \quad (1)$$

The 2D Hamming filter is defined as the outer product of two 1D Hamming filters, where  $\alpha = 25/46$  and  $N$  represents the number of samples in the signal. However, unlike in [35], we do not utilize the Hamming filter as a window function in the spatial domain. Instead, we directly apply the Hamming filter in the frequency domain as a pointwise multiplication. As a result, our Hamming filter possesses a truly infinite and periodic nature in the spatial domain, effectively preventing spectral leakage artifacts.

## 4. Experiments

Our evaluation consists of three main aspects. Firstly, we visually demonstrate the presence of aliasing artifacts following downsampling, as well as spectral artifacts resulting from FLC Pooling [12]. Secondly, we assess the performance of state-of-the-art models trained using standard techniques against both FLC Pooling and our new ASAP. Through this evaluation, we showcase that ASAP exhibits superior inherent robustness against common corruptions and adversarial attacks.

Lastly, we evaluate our ASAP network in combination with adversarial training and demonstrate its ability to prevent catastrophic overfitting during FGSM adversarial training, similar to the performance of FLC Pooling [12]. More-

Table 1. Mean and standard deviation of the aliasing measure [13] and power spectrum difference measured via KL divergence after downsampling with different downsampling methods over 1000 images of CIFAR10. FLC pooling [12] as well as our ASAP do not suffer from aliasing. Hence, aliasing is zero.

Name	Aliasing ( $\downarrow$ )	Power Spectrum difference ( $\downarrow$ )
MaxPooling	$0.26 \pm 0.30$	$174 \pm 18469$
Striding	$0.17 \pm 0.17$	$233 \pm 29669$
FLC pooling[12]	0	$240 \pm 29978$
ASAP (ours)	0	$185 \pm 27424$

over, ASAP is able to achieve a consistent increase in robustness against complex adversaries, like PGD [25], compared to FLC Pooling.

### 4.1. Artifact Representation

Firstly, we demonstrate the recognition of aliasing in the spatial domain. Aliasing occurs when high-frequency components overlap in the frequency domain, resulting in grid artifacts in the spatial domain as shown in Figure 4. The leftmost image represents the original image before downsampling, while the middle and right images depict the downsampled versions by a factor of eight. The middle image, downsampled without any anti-aliasing, exhibits prominent grid artifacts, particularly noticeable in the zebra’s fur and around its head. In contrast, the image downsampled using an anti-aliasing mechanism called FLC pooling [12], shows an aliasing-free downsampled version (rightmost image in Figure 4).

However, upon closer examination of the quality and stability of the FLC pooled image, we discover that it is still susceptible to spectral leakage artifacts. These artifacts manifest as ringing artifacts, predominantly visible around the zebra’s head in Figure 1.

Furthermore, these artifacts become more pronounced in Figure 5 in the second row. Here, FLC pooling [12] is employed for downsampling, successfully preventing aliasing. However, it remains prone to spectral artifacts, particularly noticeable at the edges of the heart after four downsampling steps (third column). These artifacts occur due to the application of a rectangular box filter in the frequency domain. The finite filter in the frequency domain transforms into an infinite sinc filter in the spatial domain, resulting in the appearance of ringing artifacts, as depicted in Figure 1, 4, and 5.

To mitigate these artifacts, we apply a Hamming filter, as described in Section 3. By implementing the Hamming filter prior to the transformation into the spatial domain, the

Table 2. Mean accuracy and standard deviation on clean samples, perturbed samples with FGSM [9] and APGD [2] as well as corrupted samples [16] for several state-of-the-art models (five different random seeds) trained without adversarial training on CIFAR-10. We clearly can see, that our ASAP which neither suffers from aliasing nor from spectral artifacts, is more robust against common corruptions than the baseline as well as FLC Pooling [12]. Further, ASAP can achieve higher clean as well as robust accuracy in most cases.

Name	Acc@1	FGSM	APGD	Corruptions
ResNet-18 [15]	93.03 ± 0.13	78.62 ± 0.28	72.49 ± 0.67	76.93 ± 0.45
FLC nonorm [12]	93.12 ± 0.19	78.92 ± 0.26	74.17 ± 0.60	78.59 ± 0.29
ASAP (ours)	<b>93.12 ± 0.25</b>	<b>79.08 ± 0.43</b>	<b>75.06 ± 0.76</b>	<b>78.68 ± 0.19</b>
WideResNet-50-2 [39]	94.33 ± 0.13	<b>77.92 ± 0.64</b>	69.36 ± 1.20	77.08 ± 0.38
FLC nonorm [12]	94.33 ± 0.20	75.41 ± 0.41	66.30 ± 0.87	79.33 ± 0.43
ASAP (ours)	<b>94.51 ± 0.17</b>	77.22 ± 0.89	<b>71.24 ± 1.86</b>	<b>79.90 ± 0.37</b>
Preact-ResNet-18	92.91 ± 0.13	<b>79.74 ± 0.16</b>	<b>68.75 ± 0.54</b>	75.67 ± 0.46
FLC nonorm [12]	92.91 ± 0.17	77.68 ± 0.35	65.95 ± 1.97	78.34 ± 0.61
ASAP (ours)	<b>93.19 ± 0.08</b>	77.88 ± 0.37	67.98 ± 0.90	<b>78.91 ± 0.70</b>
MobileNet-v2 [31]	<b>94.72 ± 0.09</b>	80.04 ± 0.43	75.55 ± 0.59	71.33 ± 0.90
FLC nonorm [12]	94.30 ± 0.18	80.81 ± 0.20	77.65 ± 0.53	71.43 ± 0.38
ASAP (ours)	94.49 ± 0.05	<b>81.12 ± 0.28</b>	<b>78.24 ± 0.44</b>	<b>71.57 ± 0.52</b>

spectral leakage artifacts disappear (third row of Figure 5).

**Numerical Stability.** However, we encountered a challenge in stabilizing the transformation into the frequency domain. The third row of images in Figure 5 demonstrates our downsampling approach with a Hamming filter, but the heart shape appears slightly shifted to the right. This is a result of performing the Fast Fourier Transform (FFT) on 2D data in PyTorch, which leverages the separability of the Fourier Transform. Typically, the FFT is computed first in one direction (vertically) and then in the other direction (horizontally). Due to numerical instabilities, this process can introduce shifts in the image after multiple transform applications. To address this, we implemented stabilization techniques to achieve centered aliasing and spectral artifact-free downsampling (fourth row of Figure 5), by transposing the image before every other FFT, such that row-first and column-first FFT are applied in an alternating manner.

Finally, we compare the power spectrum of the final downsampled images in the last column of Figure 5. While MaxPooling suppresses the frequency spectrum, all the aliasing-free downsampling methods successfully retain information in the low, middle, and high-frequency regions. Nonetheless, FLC pooling introduces slightly more varied frequency components, which can be attributed to the additional ringing artifacts resulting from spectral leakage artifacts after transformation. Figure 2 demonstrates a comprehensive example of the power spectrum after downsampling. The first column shows the original image with the full power spectrum. Each column presents a different downsampling technique with the qualitative result after downsampling in the first row and the resulting power

spectrum in the second row. Our ASAP is the only method that obtains a similar power spectrum than the original image. Further, we evaluate the aliasing measure proposed in [13] on the different downsampling methods as well as the difference in power spectrum over 1000 CIFAR10 images. Table 1 demonstrates that our ASAP is the only method that is aliasing-free while maintaining a similar power spectrum.

## 4.2. Native Robustness

To evaluate the native robustness of our proposed ASAP, we conducted experiments using two different datasets. For the low-resolution dataset, CIFAR-10 [24], we trained multiple networks with five different random seeds per network architecture. All networks were trained with the same set of hyperparameters: 150 epochs, a batch size of 256, a cosine learning rate schedule with a maximum learning rate of 0.2 and a minimum of 0, a momentum of 0.9, and a weight decay of 0.002. We utilized the LabelSmoothingLoss with a label smoothing factor of 0.1 as the loss function, and the optimizer used was Stochastic Gradient Descent (SGD).

Table 2 presents the results of the different networks trained on CIFAR-10 using clean training. It is evident that our ASAP achieves the highest native robustness against common corruptions across all architectures. Compared to the baseline method, our ASAP achieves an accuracy improvement of over 3% on corrupted data. Furthermore, the models employing our ASAP consistently achieve higher accuracy on clean data, except for MobileNetV2. Similarly, under the complex APGD attack [2], our ASAP networks demonstrate superior performance, with an accuracy

Table 3. Clean and robust accuracy for several state-of-the-art models trained without adversarial training on ImageNet-1k. Attacks are done with an epsilon of  $\epsilon = 1/255$ . We clearly can see, that our ASAP which neither suffers from aliasing nor from spectral artifacts, is natively more robust against complex adversaries like APGD [2] and common corruptions.

Name	Acc@1	Acc@5	APGD	FGSM	Corruptions@1	Corruptions@5
ResNet-18 [15]	<b>69.56</b>	89.09	0.01	21.20	34.37	54.66
FLC [12]	69.16	88.91	<b>0.32</b>	35.21	40.19	61.82
ASAP (ours)	69.53	<b>89.11</b>	0.31	<b>36.44</b>	<b>40.33</b>	<b>61.99</b>
ResNet-50 [15]	75.85	92.88	0.07	36.00	40.80	61.18
FLC [12]	<b>77.13</b>	93.44	0.53	<b>59.05</b>	50.51	71.59
ASAP (ours)	77.12	<b>93.45</b>	<b>0.67</b>	57.72	<b>50.76</b>	<b>71.87</b>
ResNet-101 [15]	77.25	93.54	0.04	38.66	46.09	67.01
FLC [12]	<b>78.16</b>	93.95	1.26	58.49	52.91	73.72
ASAP (ours)	78.11	<b>94.12</b>	<b>1.32</b>	<b>59.56</b>	<b>53.13</b>	<b>73.99</b>
Wide-ResNet-50-2 [39]	78.29	94.03	0.28	37.74	45.23	65.75
FLC [12]	79.67	<b>94.74</b>	<b>0.64</b>	<b>54.00</b>	48.48	69.22
ASAP (ours)	<b>79.68</b>	94.71	0.61	53.43	<b>48.99</b>	<b>69.63</b>
MobileNet-v2 [31]	<b>71.36</b>	<b>90.12</b>	0.00	14.29	34.13	54.43
FLC [12]	66.81	87.72	0.26	25.21	34.70	55.64
ASAP (ours)	66.83	87.71	<b>0.29</b>	<b>25.58</b>	<b>35.10</b>	<b>56.18</b>

Table 4. Accuracy for several state-of-the-art models trained with FGSM adversarial training [9] on CIFAR-10. We report adversarial robustness against FGSM [9] and PGD [25] with an  $\epsilon$  of 8/255. We clearly see, that our ASAP which neither suffers from aliasing nor from spectral artifacts, is also more robust in combination with adversarial training. Especially when confronted with unseen complex adversaries our ASAP shows superior performance to the previous FLC pooling [12].

Name	Acc@1	FGSM	PGD
ResNet-18 [15]	78.85 ± 1.74	34.49 ± 2.68	21.14 ± 14.88
FLC nonorm [12]	<b>79.77 ± 0.49</b>	34.37 ± 1.07	32.23 ± 0.68
ASAP (ours)	79.59 ± 0.64	<b>35.13 ± 0.75</b>	<b>32.65 ± 0.59</b>
Wide-ResNet-50-2 [39]	79.42 ± 0.34	39.18 ± 7.15	23.36 ± 16.35
FLC nonorm [12]	82.94 ± 0.89	39.23 ± 0.32	29.69 ± 11.81
ASAP (ours)	<b>83.63 ± 0.14</b>	<b>39.67 ± 0.28</b>	<b>37.62 ± 0.24</b>
PreAct-ResNet-18	77.92 ± 0.19	31.74 ± 0.56	32.52 ± 0.35
FLC nonorm [12]	<b>79.99 ± 0.09</b>	<b>36.39 ± 0.74</b>	33.15 ± 0.19
ASAP (ours)	79.91 ± 0.17	36.25 ± 0.20	<b>33.20 ± 0.14</b>

improvement of over 2.5% for all networks except PreAct-ResNet-18. In the case of the simple FGSM attack, our ASAP networks outperform the other networks in half of the cases, while the baseline achieves higher robust accuracy for two networks. Overall, our ASAP networks consistently exhibit increased native robustness compared to both the baseline downsampling method and FLC pooling [12].

Due to computational limitations, we only trained one network per architecture on the higher-resolution ImageNet-1k dataset [4]. The baseline networks utilized

the pre-trained weights provided by PyTorch, while for FLC pooling and our ASAP, we followed the training procedures suggested by the original authors of each network.

Table 3 presents the performance of each network on clean, perturbed, and corrupted versions of the ImageNet-1k dataset. Similar to CIFAR-10, our ASAP networks consistently achieve superior native robustness against common corruptions. Compared to the baseline models, our ASAP can improve the accuracy on corrupted data by over 10% (ResNet-50). Moreover, under adversarial attacks, our

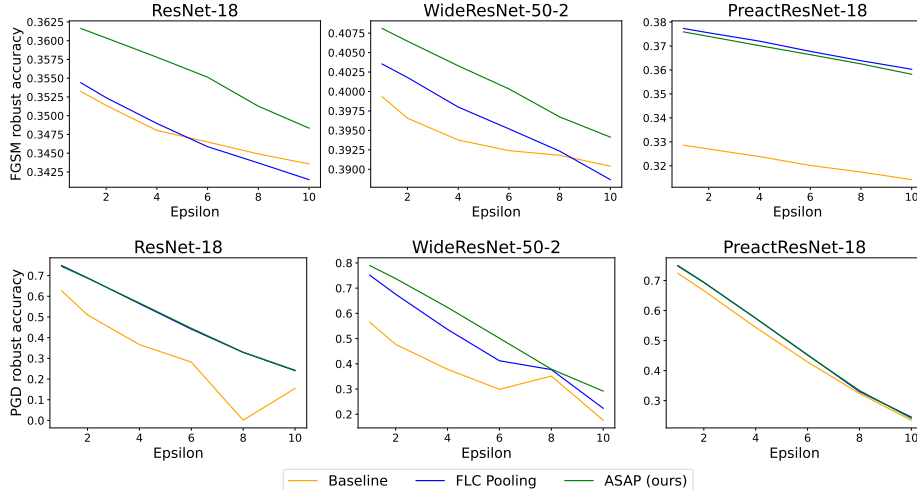


Figure 6. Evaluation of networks trained with FGSM adversarial training on FGSM [9] (top) and PGD [25] (bottom) adversaries with different budgets of  $\epsilon$ . Our ASAP consistently exhibits higher robust accuracy on all architectures, adversarial attacks and  $\epsilon$  than the baseline.

ASAP achieves significantly higher accuracies compared to the baseline. When compared to FLC pooling, our ASAP outperforms it in three out of five cases, with only slight performance degradation (0.03% under APGD attack and 1.33% under FGSM attack) in the remaining two cases.

### 4.3. Catastrophic Overfitting

Furthermore, we conducted an evaluation of our ASAP in conjunction with simple FGSM adversarial training [9]. For this evaluation, we trained each model architecture with FGSM adversarial training using three different random seeds. All hyperparameters were kept consistent across the architectures and downsampling methods. Each network underwent 300 training epochs with a batch size of 512 and a cycling learning rate schedule ranging from a maximum of 0.2 to a minimum of 0. The momentum was set to 0.9, and weight decay was set to 0.0005. We employed CrossEntropyLoss as the loss function and utilized Stochastic Gradient Descent (SGD) as the optimizer. The budget for the adversaries during training was set to  $\epsilon = 8/255$ .

The evaluation results in Table 4 demonstrate that our ASAP, similar to FLC pooling [12], achieves higher robustness against adversarial attacks. Particularly against more complex adversaries like PGD [25], our ASAP consistently outperforms the baseline and FLC pooling. Furthermore, our ASAP exhibits superior robustness against FGSM attacks and higher clean accuracy compared to the baseline (up to 5% improvement against FGSM attacks and up to 4% improvement on clean data).

Additionally, we assessed the behavior of our ASAP under different budget settings of  $\epsilon$ . Figure 6 displays the mean robust accuracy trend across each architecture, varying the budget of  $\epsilon$ . It is evident that our ASAP consistently

outperforms the baseline. Moreover, ASAP demonstrates superior performance compared to FLC pooling for ResNet and WideResNet, while for PreActResNet, both pooling methods achieve nearly equivalent results.

## 5. Discussion

Our ASAP achieves higher native robustness against common corruptions as well as adversarial attacks. Still, we need to perform additional operations to transform into from the spatial into the frequency domain and vice versa. Hence, we achieve this native robustness with increased computational effort. Yet, including additional data augmentation for robustness against common corruptions, which increases the number of samples that need to be learned or even adversarial training takes much longer. We refer here to previous work, in which the authors also need to include the transformation into the frequency domain, FLC pooling [12]. Their analysis shows that adding this additional transformation only increases the training time by a factor of two while using more sophisticated adversarial training which achieves similar performance increases the training time by at least eight or even almost sixteen. Further, they state that incorporating additional data like *ddpm* increases the training time by a factor of twenty. Hence, we believe that including additional FFTs into the network results in much less training time while achieving high native robustness as well as robustness after adversarial training.

## 6. Conclusion

We introduce ASAP, Aliasing and Spectral Artifact-free Pooling, an innovative downsampling approach that effectively eliminates both aliasing and spectral artifacts.



Through extensive qualitative analysis, we illustrate that ASAP successfully avoids both aliasing and spectral leakage artifacts. Additionally, we address the issue of FFT transformation stability in the frequency domain to prevent shifts caused by repeated FFT execution. Our quantitative evaluation showcases that ASAP exhibits superior native robustness against common corruptions and adversarial attacks while maintaining high accuracy on clean data. Moreover, when combined with simple FGSM adversarial training, ASAP sustains high levels of robustness and accuracy by preventing catastrophic overfitting. We believe that these insights emphasize the importance of conducting thorough analyses of network components to enhance the native robustness of neural networks.

## References

- [1] Yair Carmon, Aditi Raghunathan, Ludwig Schmidt, John C Duchi, and Percy S Liang. Unlabeled data improves adversarial robustness. *Advances in Neural Information Processing Systems*, 32, 2019. 3
- [2] Francesco Croce and Matthias Hein. Mind the box:  $l_1$ -apgd for sparse adversarial attacks on image classifiers. In *ICML*, 2021. 2, 6, 7
- [3] Ekin D Cubuk, Barret Zoph, Dandelion Mane, Vijay Vasudevan, and Quoc V Le. Autoaugment: Learning augmentation policies from data. *arXiv preprint arXiv:1805.09501*, 2018. 3
- [4] Jia Deng, Wei Dong, Richard Socher, Li-Jia Li, Kai Li, and Li Fei-Fei. Imagenet: A large-scale hierarchical image database. In *2009 IEEE Conference on Computer Vision and Pattern Recognition*, pages 248–255, 2009. 7
- [5] Ricard Durall, Margret Keuper, and Janis Keuper. Watch your up-convolution: Cnn based generative deep neural networks are failing to reproduce spectral distributions, 2020. 3
- [6] Logan Engstrom, Andrew Ilyas, Hadi Salman, Shibani Santurkar, and Dimitris Tsipras. Robustness (python library), 2019. 3
- [7] Robert Geirhos, Patricia Rubisch, Claudio Michaelis, Matthias Bethge, Felix A Wichmann, and Wieland Brendel. Imagenet-trained cnns are biased towards texture; increasing shape bias improves accuracy and robustness. *arXiv preprint arXiv:1811.12231*, 2018. 3
- [8] Rafael C Gonzales and Paul Wintz. *Digital image processing*. Addison-Wesley Longman Publishing Co., Inc., 1987. 3
- [9] Ian J. Goodfellow, Jonathon Shlens, and Christian Szegedy. Explaining and harnessing adversarial examples, 2015. 2, 3, 6, 7, 8
- [10] Sven Gowal, Chongli Qin, Jonathan Uesato, Timothy Mann, and Pushmeet Kohli. Uncovering the limits of adversarial training against norm-bounded adversarial examples, 2021. 3
- [11] Sven Gowal, Sylvestre-Alvise Rebuffi, Olivia Wiles, Florian Stimberg, Dan Andrei Calian, and Timothy A Mann. Improving robustness using generated data. *Advances in Neural Information Processing Systems*, 34, 2021. 3
- [12] Julia Grabinski, Steffen Jung, Janis Keuper, and Margret Keuper. Frequencylowcut pooling—plug & play against catastrophic overfitting. In *European Conference on Computer Vision*, 2022. 1, 2, 3, 4, 5, 6, 7, 8
- [13] Julia Grabinski, Janis Keuper, and Margret Keuper. Aliasing and adversarial robust generalization of cnns. *Machine Learning*, pages 1–27, 2022. 1, 2, 3, 5, 6
- [14] Richard W Hamming and Samuel D Stearns. Digital filters. *IEEE Transactions on Systems, Man, and Cybernetics*, 9(1):67–67, 1979. 3
- [15] Kaiming He, Xiangyu Zhang, Shaoqing Ren, and Jian Sun. Deep residual learning for image recognition. In *Proceedings of the IEEE conference on computer vision and pattern recognition*, pages 770–778, 2016. 6, 7
- [16] Dan Hendrycks and Thomas Dietterich. Benchmarking neural network robustness to common corruptions and perturbations. *Proceedings of the International Conference on Learning Representations*, 2019. 2, 3, 6
- [17] Dan Hendrycks, Norman Mu, Ekin D. Cubuk, Barret Zoph, Justin Gilmer, and Balaji Lakshminarayanan. AugMix: A simple data processing method to improve robustness and uncertainty. *Proceedings of the International Conference on Learning Representations (ICLR)*, 2020. 3
- [18] Jonathan Ho, Ajay Jain, and Pieter Abbeel. Denoising diffusion probabilistic models. *Advances in Neural Information Processing Systems*, 33:6840–6851, 2020. 3
- [19] Md Tahmid Hossain, Shyh Wei Teng, Guojun Lu, Mohammad Arifur Rahman, and Ferdous Sohel. Anti-aliasing deep image classifiers using novel depth adaptive blurring and activation function. *Neurocomputing*, 536:164–174, 2023. 3
- [20] Bernd Jähne. *Digital image processing*. Springer Science & Business Media, 2005. 3
- [21] Steffen Jung and Margret Keuper. Spectral distribution aware image generation. In *Proceedings of the AAAI conference on artificial intelligence*, volume 35, pages 1734–1742, 2021. 3
- [22] Tero Karras, Miika Aittala, Samuli Laine, Erik Härkönen, Janne Hellsten, Jaakko Lehtinen, and Timo Aila. Alias-free generative adversarial networks. *Advances in Neural Information Processing Systems*, 34, 2021. 3
- [23] Klim Kireev, Maksym Andriushchenko, and Nicolas Flammarion. On the effectiveness of adversarial training against common corruptions. In James Cussens and Kun Zhang, editors, *Proceedings of the Thirty-Eighth Conference on Uncertainty in Artificial Intelligence*, volume 180 of *Proceedings of Machine Learning Research*, pages 1012–1021. PMLR, 01–05 Aug 2022. 3
- [24] Alex Krizhevsky, Geoffrey Hinton, et al. Learning multiple layers of features from tiny images. 2009. 6
- [25] Alexey Kurakin, Ian Goodfellow, and Samy Bengio. Adversarial machine learning at scale, 2017. 2, 3, 5, 7, 8
- [26] Qiufu Li, Linlin Shen, Sheng Guo, and Zhihui Lai. Wavecnet: Wavelet integrated cnns to suppress aliasing effect for noise-robust image classification. *IEEE Transactions on Image Processing*, 30:7074–7089, 2021. 3
- [27] KM Muraleedhara Prabhu. *Window functions and their applications in signal processing*. Taylor & Francis, 2014. 3

- [28] Rahul Rade and Seyed-Mohsen Moosavi-Dezfooli. Helper-based adversarial training: Reducing excessive margin to achieve a better accuracy vs. robustness trade-off. In *ICML 2021 Workshop on Adversarial Machine Learning*, 2021. 3
- [29] Sylvestre-Alvise Rebuffi, Sven Gowal, Dan A. Calian, Florian Stumberg, Olivia Wiles, and Timothy Mann. Fixing data augmentation to improve adversarial robustness, 2021. 3
- [30] Jérôme Rony, Luiz G Hafemann, Luiz S Oliveira, Ismail Ben Ayed, Robert Sabourin, and Eric Granger. Decoupling direction and norm for efficient gradient-based l2 adversarial attacks and defenses. In *Proceedings of the IEEE/CVF Conference on Computer Vision and Pattern Recognition*, pages 4322–4330, 2019. 3
- [31] Mark Sandler, Andrew Howard, Menglong Zhu, Andrey Zhmoginov, and Liang-Chieh Chen. Mobilenetv2: Inverted residuals and linear bottlenecks. In *Proceedings of the IEEE conference on computer vision and pattern recognition*, pages 4510–4520, 2018. 6, 7
- [32] Vikash Schwag, Saeed Mahloujifar, Tinashe Handina, Sihui Dai, Chong Xiang, Mung Chiang, and Prateek Mittal. Improving adversarial robustness using proxy distributions, 2021. 3
- [33] John L Semmlow and Benjamin Griffel. *Biosignal and medical image processing*. CRC press, 2021. 3
- [34] C.E. Shannon. Communication in the presence of noise. *Proceedings of the IRE*, 37(1):10–21, 1949. 4
- [35] Nergis Tomen and Jan C van Gemert. Spectral leakage and rethinking the kernel size in cnns. In *Proceedings of the IEEE/CVF International Conference on Computer Vision*, pages 5138–5147, 2021. 3, 5
- [36] Yisen Wang, Difan Zou, Jinfeng Yi, James Bailey, Xingjun Ma, and Quanquan Gu. Improving adversarial robustness requires revisiting misclassified examples. In *International Conference on Learning Representations*, 2020. 3
- [37] Eric Wong, Leslie Rice, and J. Zico Kolter. Fast is better than free: Revisiting adversarial training. In *International Conference on Learning Representations*, 2020. 3
- [38] Dongxian Wu, Shu-Tao Xia, and Yisen Wang. Adversarial weight perturbation helps robust generalization. *Advances in Neural Information Processing Systems*, 33:2958–2969, 2020. 3
- [39] Sergey Zagoruyko and Nikos Komodakis. Wide residual networks. *arXiv preprint arXiv:1605.07146*, 2016. 6, 7
- [40] Hongyang Zhang, Yaodong Yu, Jiantao Jiao, Eric P. Xing, Laurent El Ghaoui, and Michael I. Jordan. Theoretically principled trade-off between robustness and accuracy. In *International Conference on Machine Learning*, 2019. 3
- [41] Richard Zhang. Making convolutional networks shift-invariant again. In *International conference on machine learning*, pages 7324–7334. PMLR, 2019. 1, 2, 3, 4
- [42] Xueyan Zou, Fanyi Xiao, Zhiding Yu, and Yong Jae Lee. Delving deeper into anti-aliasing in convnets. In *BMVC*, 2020. 1, 2, 3, 4